Residual Stresses Generation in Ultra-Thick Components for Wind Turbine Blades

Struzziero, Giacomo; Teuwen, Julie J.E.

DOI
10.1016/j.procir.2019.09.002

Publication date
2019

Document Version
Final published version

Published in
Proceedings of 2nd CIRP Conference on Composite Material Parts Manufacturing, Sheffield (UK), 2019

Available online at www.sciencedirect.com

ScienceDirect

Procedia CIRP 85 (2019) 8–12

www.elsevier.com/locate/procedia

2nd CIRP Conference on Composite Material Parts Manufacturing (CIRP-CCMPM 2019)

Residual Stresses Generation in Ultra-Thick Components for Wind Turbine Blades

G. Struzziero[a]*, J.J.E. Teuwen[a]

[a]*Faculty of Aerospace, Aerospace Manufacturing Technologies, Delft University of Technology, Delft, 2629 HS, Netherlands*

* Corresponding author. *E-mail address:* G.Struzziero@tudelft.nl

Abstract

The present paper investigates the generation of cure induced residual stresses during the cure stage of the Vacuum Assisted Resin Transfer Moulding (VARTM) process for the fabrication of ultra-thick components (i.e. 105 mm) for wind turbine blades manufacturing (i.e. root insert). The viscous-elastic material characterisation of the Airstone 780E epoxy resin mixed with the 785H Hardener has been undertaken and the corresponding coupled thermo-mechanical simulation has been implemented using a commercial FE solver. The finding points out that the level of residual stresses generated during the cure stage leads to a spring-in of about 1.3 cm when Manufacturer Recommended Cure Cycle is applied and that improvements in both spring-in and cure time can be obtained by applying different cure cycles.

Keywords: Composite; VARTM; Thermo-mechanical properties; Springback; Residual stress

1. Introduction

The curing stage of composite manufacturing presents several challenges to produce components that comply with the high quality requirements and stringent delivery time. A poorly designed curing stage can lead to formation of cure induced defects (e.g. residual stresses) that lower performances of the component and in more severe cases lead to rejection of the part with consequences on production cost and sustainability. The matter becomes even more complex when dealing with thick and ultra-thick components. Structural components for wind industry fall into the ultra-thick category with the root-insert reaching about 100 mm thickness. Within this framework it is important to predict beforehand the generation of residual stresses and adjust design parameters before going into production to minimise scrapped parts and maximise performances. Residual stresses arise during curing stage due to resin shrinkage and anisotropy in coefficient of thermal expansion and tool-part interaction [1, 2]. The occurrence of compressive and tensile residual stresses within the manufactured parts leads to spring-in and warpage after mould removal [3, 4]. However, it has been shown that residual stresses can also be beneficial (i.e. longitudinal and transverse tensile strength [5, 6] and delamination properties [7, 8]) for mechanical performances but also detrimental for in-plane shear strength [8, 9] therefore their development during curing needs to be quantified when considering mechanical performances of in-service parts. Furthermore, it has been shown that Manufacturer Recommended Cure Cycles (MRCC) do not lead to optimal solutions [10-13] and that different cure cycles can induce different residual stresses within the part [14-16].

In the present paper the viscous elastic properties of the Airstone 780E/785H epoxy system will be characterised and constitutive materials models built. A coupled thermo-mechanical FE model of the Vacuum Assisted Resin Transfer Moulding (VARTM) for manufacturing of the root insert of a wind turbine blade will be performed to predict spring-in of the part. The paper constitutes the starting point for a multi-objective optimisation work which focuses on the minimisation of cure time and residual stresses by identifying optimal cure cycles.

10.1016/j.procir.2019.09.002

Nomenclature

$E_l\ [GPa]$	Composite longitudinal Young's modulus
$E_t\ [GPa]$	Composite transverse Young's modulus
$G_{12}\ [GPa]$	Composite shear modulus
ν_{12}	Composite in-plane Poisson's ratio
$E_r\ [GPa]$	Resin Young's modulus
$G_r\ [GPa]$	Resin shear modulus
ν_r	Resin Poisson's ratio
$E_{lf}[GPa]$	Fibre longitudinal Young's modulus
$E_{tf}[GPa]$	Fibre transverse Young's modulus
$G_f\ [GPa]$	Fibre shear modulus
ν_{12f}	Fibre Poisson's ratio
$\mathrm{a_l}\ [°C^{-1}]$	Composite longitudinal CTE
$\mathrm{a_t}\ [°C^{-1}]$	Composite transverse CTE
$\mathrm{a_r}\ [°C^{-1}]$	Resin CTE
$\mathrm{a_{lf}}\ [°C^{-1}]$	Fibre longitudinal CTE
$\mathrm{a_{tf}}\ [°C^{-1}]$	Fibre transverse CTE
γ_l	Composite longitudinal shrinkage
γ_t	Composite transverse shrinkage
γ_r	Resin linear shrinkage
$E_{glass}\ [GPa]$	Resin modulus at glass state
$E_{rub}\ [GPa]$	Resin modulus at rubber state
$T_g\ [°C]$	Glass transition temperature
$E_{rub\alpha}[GPa]$	Resin modulus dependency on degree of cure
A	Exponential parameter
$C\ [°C^{-1}]$	Breadth of transition
$\sigma\ [°C]$	Temperature shift
$a_r\ [°C^{-1}]$	Resin CTE
$a_{glass}\ [°C^{-1}]$	Resin CTE at glass state
$a_{rub}\ [°C^{-1}]$	Resin CTE at rubber state
ν_{glass}	Resin Poisson's ratio at glass state
ν_{rub}	Resin Poisson's ratio at rubber state

2. Sub-material models

The materials used in this study are a non-crimp triaxial E-glass fibres fabric and the two component Airstone™ 780E epoxy resin and 785H hardener system [17]. The thermo-chemical model for the resin system under study including cure kinetics, specific heat and thermal conductivity have been presented and validated elsewhere [13] and therefore not reported here.

The mechanical properties of the composite can be implemented by applying micro-mechanics law [18] accounting for the contribution from fibres and resin. The longitudinal modulus of the composite material in the fibre (E_l), transverse (E_t), shear (G_{12}) directions and the in-plane Poisson's ratio (ν_{12}) are as follows:

$$E_l = v_f E_{lf} + (1 - v_f) E_r \tag{1}$$

$$E_t = \frac{E_r}{1-\sqrt{v_f}\left(1-\frac{E_r}{E_{tf}}\right)} \tag{2}$$

$$G_{12} = \frac{G_r}{1-\sqrt{v_f}\left(1-\frac{G_r}{G_f}\right)} \tag{3}$$

$$\nu_l = v_f \nu_{12f} + (1 - v_f)\nu_r \tag{4}$$

The modulus of the resin has been characterised by Dynamic Mechanical Analysis (DMA) tests. Four suitable samples for the DMA tests have been partially cured (i.e. 78%, 85%, 90% and 98%) to provide a degree of cure sensitivity to the model and tested with 1Hz frequency and a 2 °C/min ramp rate. To obtain the DMA samples, four partially cured pure resin plates have been manufactured to achieve different levels of degree of cure; four (IV) different cure cycles have been adopted; (I) 45 minutes at 70 °C, (II) 95 minutes at 70 °C, (III) 255 minutes at 70 °C and (IV) 135 minutes at 110 °C. The degree of cure of each plate has been measured by means of Differential Scanning Calorimetry (DSC) analysis. The test prescribed a quick ramp up at 10 °C/min from 10 °C. The test was interrupted after glass transition occurred. The glass transition temperature was therefore identified and according to the model reported in [13] the corresponding degree of cure was obtained.

The coefficient of thermal expansion (CTE) of the composite can be determined by applying micromechanics law [19]:

$$a_l = \frac{(1-v_f)E_r a_r + v_f E_{lf} a_{lf}}{(1-v_f)E_r + v_f E_{lf}} \tag{5}$$

$$a_t = (1 - v_f)a_r + v_f a_{tf} + (1 - v_f)a_r \nu_r + \nu_{12f} a_{lf} v_f - \nu_{12} a_l \tag{6}$$

The characterisation of the resin CTE has also been undergone by means of Thermal Mechanical Analysis (TMA). The anisotropic shrinkage of the composite can be modelled as follows:

$$\gamma_l = \frac{(1-v_f)E_r \gamma_r}{(1-v_f)E_r + v_f E_{lf}} \tag{7}$$

$$\gamma_t = (1 - v_f)\gamma_r + (1 - v_f)\gamma_r \nu_r - \nu_{12f}\gamma_l \tag{8}$$

The thermo-mechanical properties of E-glass fibres are available in literature [20].

3. Coupled thermo-mechanical analysis of the cure stage

The coupled thermo-mechanical model to predict residual stresses was developed within the FE solver Marc.Mentat. The process modelled is VARTM. The three dimensional 8-nodes composite brick elements with element type 149 according to the Marc library were implemented. The element is suitable for coupled analysis. The model represents the root insert of the wind turbine blade. The volume fibre fraction is equal to 54%, radius of curvature is 1205 mm and thickness is 105 mm. The lay-up is $[0/+45/-45]_{90}$. A cross section of the thickest part of the root insert has been considered and due to symmetry reason only half of it modelled. The FE model contains 5952 nodes and 3780 elements. Fig.1 illustrates the mesh applied. Fixed displacement boundary conditions to

avoid rigid body movement and symmetry boundary conditions have been applied. The user subroutine FORCDT has been used to apply fixed temperature boundary condition to the nodes in contact with the mould whilst UFILM subroutine has been implemented to apply convection coefficient at the vacuum bag side. The sink temperature is set at room temperature and the convection coefficient is equal to 13.7 W/m°C [21]. Fig. 2 illustrates a schematic of the model and the application of boundary conditions. Due to the application of boundary conditions the problem is reduced to 2D meaning that a cross sectional strip of the root insert is considered. The constitutive material sub-models have been implemented by means of user subroutines. The cure kinetics, specific heat and thermal conductivity models have been implemented using UCURE, USPCHT and ANKOND respectively while HOOKLW, ANEXP have been used to implement modulus, Poisson and CTE models. The model for shrinkage has been implemented using user defined tables. The equations used by the FEA to calculate the stresses are reported in [1]. The prediction of the model has been validated by means of warpage measurements of three asymmetric laminates showing good agreement.

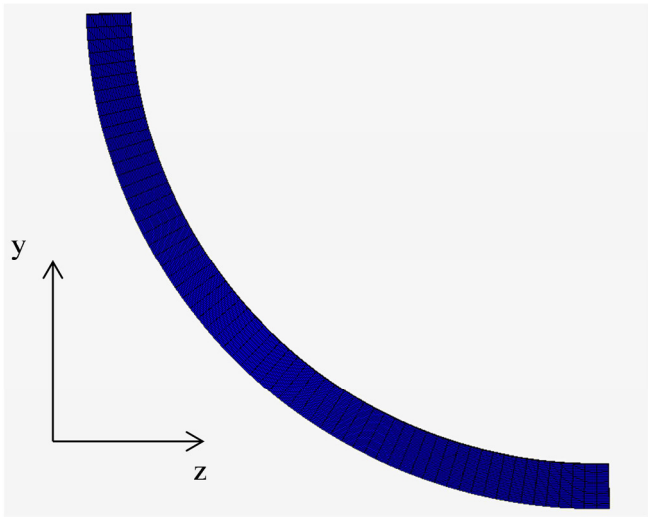

Fig. 1. Mesh applied to the part

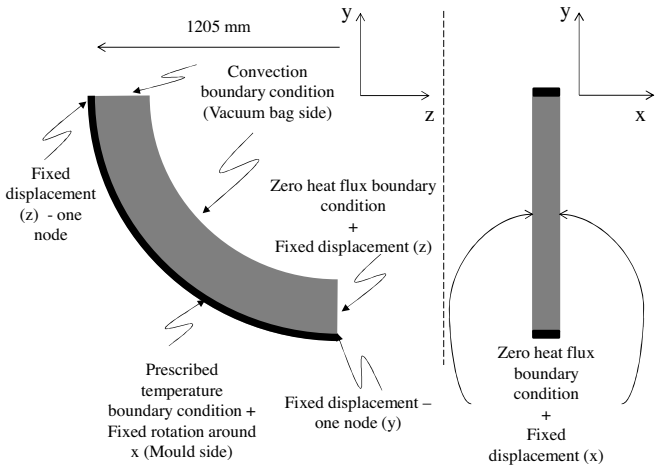

Fig. 2. Schematic of model boundary conditions

4. Results

4.1. Mechanical and thermo-mechanical properties

Fig. 3 reports the results from the DMA test for the four partially cured samples. The resin modulus show no dependence on temperature and degree of cure at the glass state, while a dependence on degree of cure is observed after transition. Therefore the following model has been used to fit the experimental data:

$$E_r = E_{rub} + E_{rub\alpha}\, exp(A\alpha) + \frac{\left(E_{glass} - E_{rub} - (E_{rub\alpha}\, exp(A\alpha))\right)}{1+exp\left(C(T-T_g-\sigma)\right)} \quad (9)$$

Compared to models found in literature [22], the current model presents an additional exponential dependence on degree of cure to describe the behaviour after transition. The additional dependence improves the accuracy of the final stress state prediction by 1%. It has to be noted that in Fig. 3 the modulus axis is reported in logarithmic scale to show the dependence on degree of cure at rubber state.

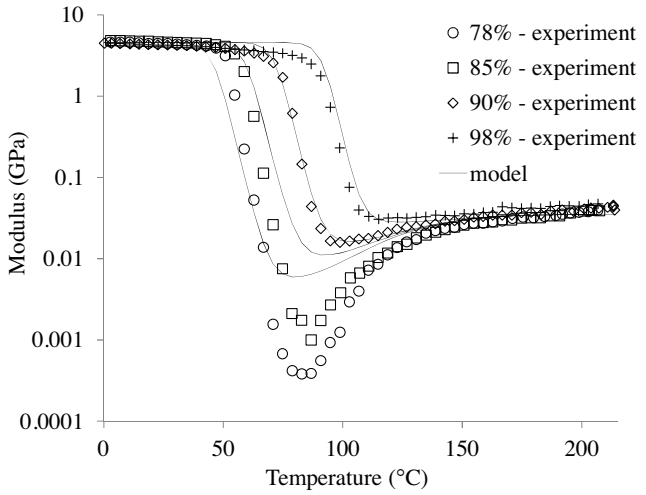

Fig. 3. DMA experimental data fitting (Modulus axis is logarithmic scale)

TMA tests have been also run to identify the rubber and glass values for the CTE of the resin. The CTE of the resin at the glass state was found to be 6 $*10^{-5}$ °C^{-1} and the value at the rubber state was equal to 1.45 $*10^{-4}$ °C^{-1}. The thermal expansion model used can be found in literature and is as follows:

$$a_r = a_{rub} + \frac{(a_{glass} - a_{rub})}{1+exp\left(C(T-T_g-\sigma)\right)} \quad (10)$$

The parameters C and σ governing the glass transition have been assumed to be as for the mechanical modulus model.

The model describing the evolution of the Poisson's ratio follows the shape of Eq. 10. The values at rubber and glass state have been taken from literature for other epoxy resin systems [23].

$$\nu_r = \nu_{rub} + \frac{(\nu_{glass} - \nu_{rub})}{1+exp\left(C(T-T_g-\sigma)\right)} \quad (11)$$

Finally, the shrinkage of the resin system was measured by measuring the change in density from the uncured to fully cured state. The total volumetric shrinkage was found to be equal to 5.4%. Table 1 reports the fitting parameters of the constitutive material models.

Table 1. Fitting parameters for modulus and CTE constitutive models

Parameters	Values	Units
E_{glass}	4.6	GPa
E_{rub}	$0.4*10^{-4}$	GPa
$E_{rub\alpha}$	1.6	kPa
A	10	
a_{glass}	$6.00*10^{-5}$	$°C^{-1}$
a_{rub}	$1.45*10^{-4}$	$°C^{-1}$
C	0.33	$°C^{-1}$
σ	10.2	°C

4.2. Simulation results

Fig. 4 shows the spring-in obtained in the part when the MRCC was applied. The MRCC for the resin under study dictates a ramp up at 0.3 °C/min to 70 °C and a dwell of 4 h at 70 °C. The cure-induced residual stresses led to a spring-in of 1.3 cm.

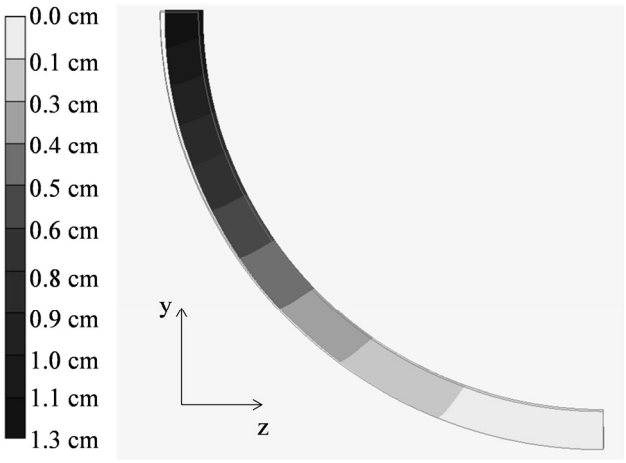

Fig. 4. Simulation results showing displacement in z direction

It is also of interest to analyse the distribution of temperature through thickness. Fig. 5 shows the temperature gradient contour plot at the moment when exothermic phenomena is fully developed at about 130 min. For the resin at hand the cure reaction kicks in even at mild temperature such as 40 °C, in addition to this the thickness involved (i.e. 105 mm) does not facilitate the dissipation of heat leading to an early occurrence of overshooting temperatures. Although the ramp rate is slow (0.3 °C/min), it is not slow enough to prevent the temperature overshooting during the ramp up to cure temperature.

The maximum temperature reached during the curing is of 145 °C which is well below the measured degradation temperature for the system that is 330 °C [17].

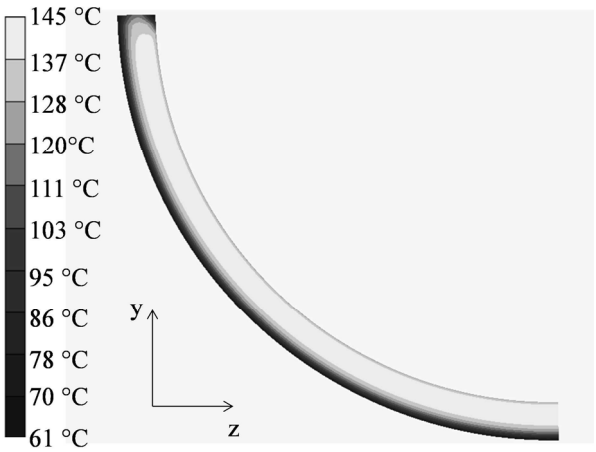

Fig. 5. Occurrence of the exothermic phenomena

Fig. 6 shows the distribution of stresses along the cross section of the root insert. The maximum tensile stress achieved is about 24 MPa. It has also to be noted that at the middle part of the thickness the highest level of stresses occur which could be due to the presence of overshoot temperatures happening in the same region. The results show that MRCC provides a non-optimal solution for the manufacturing of such component in terms of both cure time and residual stresses build-up.

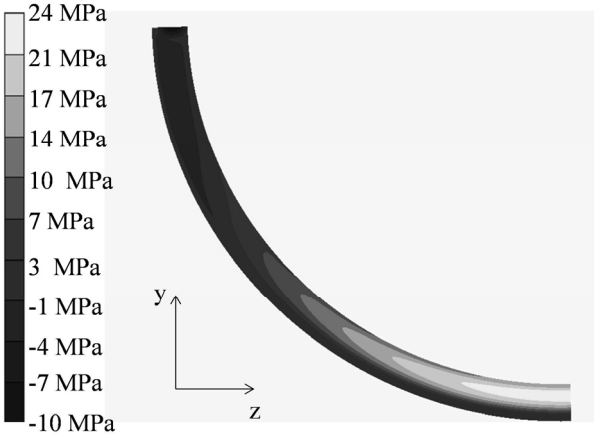

Fig. 6. Cure-induced residual stresses (σ_{zz}) generated along the cross section

To show this, a test case two dwell cure profile aiming at reducing both cure time and spring-in has been designed. The cure profile prescribes a ramp up to the first dwell at 1.0 °C/min, a first dwell temperature at 42 °C kept for 100 minutes, a second ramp rate at 1.5 °C/min, a second dwell temperature at 98 °C kept for 35 minutes and a cool down to room temperature at 0.5 °C/min. The aforementioned cure cycle produces a milder distribution of stresses which results in a final spring-in of 1.0 cm and a curing time (i.e. to reach a minimum of at least 90% degree of cure in the whole model plus cool-down) of 5h and 22 minutes. This corresponds to a 23% reduction in spring-in and 21% in process time compared to the solution obtained when the MRCC was applied. This result suggests that optimal trade-offs between the two objectives (i.e. spring-in and process time) exist and that a

multi-objective optimisation methodology can unveil optimal cure cycles to minimise them both.

5. Conclusions

In the present paper the viscous-elastic material characterisation of the Airstone 780E and Hardener 785H has been undertaken. The resin system is widely used for the manufacturing of wind turbine blades. The corresponding constitutive material models have been built and implemented in a coupled thermo-mechanical FE model and the cure stage of the VARTM process simulated. The FE model successfully led to the prediction of the spring-in of the part due to cure induced residual stresses.

Due to the thickness at play (i.e. 105 mm) the component developed significant exothermic reaction which consequently led to residual stresses build-up. The residual stresses distribution resulted in a spring-in of about 1.3 cm after demoulding when MRCC was applied. A two dwell cure cycle has been designed to reduce the spring-in. The newly designed cure profile led to a 23% reduction in spring-in and 21% process time reduction compared to MRCC solution. Future work will require further validation of the thermo-mechanical model and the implementation of the simulation analysis within a multi-objective optimisation methodology which will seek optimal cure cycles to minimise simultaneously spring-in and cure time.

Acknowledgements

Financial support from the ADEM Innovation Lab project is gratefully acknowledged.

References

[1] Bogetti TA, Gillespie JW. Process-induced stress and deformation in thicksection thermoset composite laminates. Journal of Composite Materials. 1992;26(5):626-60.

[2] Wisnom MR, Gigliotti M, Ersoy N, Campbell M, Potter KD. Mechanisms generating residual stresses and distortion during manufacture of polymer–matrix composite structures. Composites Part A: Applied Science and Manufacturing. 2006;37(4):522-9.

[3] Albert C, Fernlund G. Spring-in and warpage of angled composite laminates. Composites Science and Technology. 2002;62(14):1895-912.

[4] Çiçek KF, Erdal M, Kayran A. Experimental and numerical study of process-induced total spring-in of corner-shaped composite parts. Journal of Composite Materials. 2016;51(16):2347-61.

[5] Asp LE, Berglund LA, Talreja R. Prediction of matrix-initiated transverse failure in polymer composites. Composites Science and Technology. 1996;56(9):1089-97.

[6] Correa E, Mantič V, París F. Effect of thermal residual stresses on matrix failure under transverse tension at micromechanical level: A numerical and experimental analysis. Composites Science and Technology. 2011;71(5):622-9.

[7] Babu PR, Pradhan B. Effect of damage levels and curing stresses on delamination growth behaviour emanating from circular holes in laminated FRP composites. Composites Part A: Applied Science and Manufacturing. 2007;38(12):2412-21.

[8] Laik S, Skordos AA. Influence of residual stress on the delamination and shear response of carbon epoxy composites. ECCM15 - 15th european conference on composite materials. Venice, Italy 2012.

[9] Zhao LG, Warrior NA, Long AC. A micromechanical study of residual stress and its effect on transverse failure in polymer–matrix composites. International Journal of Solids and Structures. 2006;43(18):5449-67.

[10] Shah PH, Halls VA, Zheng JQ, Batra RC. Optimal cure cycle parameters for minimizing residual stresses in fiber-reinforced polymer composite laminates. Journal of Composite Materials. 2017;52(6):773-92.

[11] Struzziero G, Skordos AA. Multi-objective optimisation of the cure of thick components. Composites Part A: Applied Science and Manufacturing. 2017;93:126-36.

[12] Struzziero G, Skordos AA. Multi-objective optimisation of composites cure using genetic algorithms. ECCM15 - 15th European conference on composite materials. Venice, Italy 2012.

[13] Struzziero G, Teuwen JJE. Effect of convection coefficient and thickness on optimal cure cycles for the manufacturing of wind turbine components using VARTM. Composites Part A: Applied Science and Manufacturing. 2019;123:25-36.

[14] Bogetti TA, Gillespie JW. Two-Dimensional Cure Simulation of Thick Thermosetting Composites. Journal of Composite Materials. 1991;25(3):239-73.

[15] Gopal AK, Adali S, Verijenko VE. Optimal temperature profiles for minimum residual stress in the cure process of polymer composites. Composite Structures. 2000;48(1):99-106.

[16] White SR, Hahn HT. Cure cycle optimization for the reduction of processing-induced residual stresses in composite materials. Journal of Composite Materials. 1993;27(14):1352-78.

[17] AirstoneTM Infusion System Product. www.dowepoxysystems.com.

[18] Chamis C. Mechanics of Composite Materials: Past, Present, and Future. Journal of Composites, Technology and Research. 1989;11(1):3-14.

[19] Schapery RA. Thermal Expansion Coefficients of Composite Materials Based on Energy Principles. Journal of Composite Materials. 1968;2(3):380-404.

[20] Shan H, Chou T. Transverse elastic moduli of unidirectional fiber composites with fiber/matrix interfacial debonding. Composites Science and Technology. 1995;53(4):383-91.

[21] Mesogitis TS, Skordos AA, Long AC. Stochastic heat transfer simulation of the cure of advanced composites. Journal of Composite Materials. 2015;50(21):2971-86.

[22] Mesogitis TS, Skordos AA, Long AC. Stochastic simulation of the influence of fibre path variability on the formation of residual stress and shape distortion. Polymer Composites. 2017;38(12):2642-52.

[23] O'Brien DJ, Mather PT, White SR. Viscoelastic Properties of an Epoxy Resin during Cure. Journal of Composite Materials. 2001;35(10):883-904.